Rheologica Acta
https://doi.org/10.1007/s00397-018-1103-y

ORIGINAL CONTRIBUTION

A bootstrap mechanism for non-colloidal suspension viscosity

Roger I. Tanner[1] · Christopher Ness[2] · Arif Mahmud[1] · Shaocong Dai[1] · Jiyoung Moon[1]

Received: 14 May 2018 / Revised: 1 August 2018 / Accepted: 8 August 2018

Abstract
The role of friction in non-colloidal suspensions is examined with a model which splits the viscosity into a frictionless component (τ^*) plus a frictional component which depends on the ratio of the particle pressure (P) to the shear stress (τ). The model needs the input by computation of τ^* and P and a suitable choice of particle friction coefficient (μ). It can be extended to elongational flows and cases where sphere roughness is important; volume fractions up to 0.5 are considered. It is shown that friction acts in a feedback or "bootstrap" manner to increase the suspension viscosity. The analysis is also useful for deducing the friction coefficient in suspensions from experimental data. It was applied to several sets of experimental data and reasonable correlations of the viscosities were demonstrated. An example of the correlation for spheres in a silicone oil is shown for volume fractions 0.1–0.5.

Keywords Suspensions · Shear viscosity · Elongational flow · Friction

Introduction

The role of interparticle friction on the relative viscosity of non-colloidal suspensions of spheres at volume fractions (ϕ) up to about 0.5 is important, and several computational papers on the effect of friction on viscosity have been published (for example, Sierou and Brady (2002); Gallier et al (2014); Mari et al. (2014); Cheal and Ness 2018). Yet the way friction acts to increase viscosity is not quite clear, and the present work suggests a "bootstrap" feedback mechanism to account for this increase. We shall use the analysis to estimate the friction coefficient needed to explain the viscosity increases observed. We assume that the matrix fluid is Newtonian with a viscosity η_o and that inertia is negligible; the Péclet numbers in the experiments are of order 10^8.

The vast majority of studies on suspensions concentrate on simple shearing, but this is not generally sufficient to describe their rheology (Mahmud et al. 2018). Hence, in this paper, we also consider extensional flows.

We note the work of Boyer et al. (2011), who applied a compacting pressure P^p to particles in shear flow permeated by a matrix fluid. An important parameter was $I_v = \eta_o \dot{\gamma} / P^p$; this factor was also used by Gallier et al. (2014) and has been called the Leighton number (Huang et al. 2005). They measured the friction coefficient (μ) as a function of concentration, leading to a deduction of the relative viscosity η_r as a function of ϕ, the maximum packing fraction ϕ_m, and a friction coefficient $\mu^c = 0.32 + 0.38/f(\phi)$ where $\phi_m = 0.585$ and

$$f(\phi) = 1 + 0.005\phi^2 (\phi_m - \phi)^{-2} \quad (1)$$

The coefficient f was deduced for polystyrene (PS) and polymethyl methacrylate (PMMA) spheres in two matrix fluids, and with the above value of μ^c, the relative shear viscosity was expressed as

$$\eta_r = 1 + 2.5\phi (1 - \phi/\phi_m)^{-1} + \mu^c (\phi/(\phi_m - \phi))^2 \quad (2)$$

The fit of their data from $\phi = 0.3$ to 0.585 with Eq. 2 was good, but Eq. (2) does not show shear-thinning, which is very prevalent in these suspensions (Zarraga et al. 2000; Moon et al. 2015). Hence, we present below a "bootstrap" or feedback friction mechanism which allows shear thinning and which can also be used in extensional flows. Generally, the analysis is also shown to be useful in dedu

✉ Roger I. Tanner
roger.tanner@sydney.edu.au

[1] School of Aerospace, Mechanical and Mechatronic Engineering, University of Sydney, Sydney 2006, Australia

[2] Department of Chemical Engineering and Biotechnology, University of Cambridge, Cambridge CB3 0AS, UK

Published online: 24 August 2018

cing the friction coefficient variation in flowing non-colloidal suspensions.

A bootstrap mechanism

We begin with steady simple shearing and assume that the shear stress (τ) is composed of two elements—one (τ^*) is the shear stress in a frictionless suspension, and the remainder (τ^f) is due to friction. The sum of τ^* and τ^f is the total (macroscopic) shear stress. Now, τ^* can be computed but is not easily measured experimentally because truly frictionless suspensions do not exist. There are a number of computational results in the literature for frictionless suspensions and a selection is shown in Table 1.

There are some differences between these values which need to be borne in mind—these results clearly show around ± 5% variations. The computations of Mari et al. (2014) and Cheal and Ness (2018) are for a bimodal half-half mixture of spheres with a diameter ratio of 1.4:1, which causes a reduction in the value of the viscosity relative to the monodisperse case (Qi and Tanner 2011). The reduction in viscosity is caused by an increase in the maximum packing fraction of about 3% at $\phi = 0.5$ due to bimodality, leading to a drop in viscosity of order 10% relative to the monodisperse case. At lower concentrations, the effect of bimodality is less marked.

We assume that τ^f is due to friction induced by the mean particle pressure (P) forcing particle-particle contact; P is defined as $-1/3\ (\mathrm{Tr}\boldsymbol{\sigma}_p)$, where $\boldsymbol{\sigma}_p$ is the stress tensor due to the particles. It should be emphasized that P is not equal to the pressure p used to balance the momentum equation—the two can differ by any amount due to, for example, an imposed hydrostatic pressure. Hence, the value of P is equal to the P^p quantity of Boyer et al. (2011) and the P value of Cheal and Ness (2018) mentioned above and is related to the Σ stress tensor of Sierou and Brady (2002).

It is assumed that $\tau^f = k\mu P$, where k is a constant and μ is a coefficient of friction for the spheres. From the data of Cheal and Ness (2018) and subsequent computations by Ness, one can find numerical estimates of P/τ for $\phi = 0.3$, 0.4, and 0.5 as shown in Fig. 1 and in column 3 of Table 2. These computations were made for $\mu = 0$, 0.25, 0.5, 0.75, and 1.

Generally, one would expect that polystyrene spheres would have a friction coefficient of about 0.4–0.5 (Bowden and Tabor 1956); we assume here, since there is some lubrication, that the value is 0.40. Hence, in order to compare with our experiments, we have used the Cheal and Ness (2018) values of P/τ as in Fig. 1 for the entries for $\phi = 0.4$ and 0.5 in column 3 (Table 2). Support for these results can be found from the paper by Gallier et al. (2014). They show in their Figure 17 values of the normal stresses as a function of friction coefficient for $\mu = 0$ to 0.8 at $\phi = 0.4$. The increase in P/τ with μ for these data is close to linear. For $\phi = 0.1$–0.2 in Table 2, we use the values given by Sierou and Brady (2002) which assume $\mu = 0$; friction is not important at these lower concentrations (Gallier et al. 2014). For $\phi = 0.3$ from Gallier et al. (2014), we use $P/\tau = 0.20$.

With these assumptions, we find

$$\eta_r = \eta_r^* + k\,\mu\,(P/\tau)\,\eta_r \quad \text{or} \quad \eta_r = \eta_r^*/(1 - k\,\mu\,(P/\tau)) \tag{3}$$

where η_r^* is the relative viscosity for a frictionless suspension at the given volume fraction (ϕ). We use the average computed values of η_r^* from Table 1, and for $\phi = 0.1$, 0.2 values are taken from Sierou and Brady (2002).

Equation 3 shows a "bootstrap" or feedback character so often seen in frictional studies; a greater stress intensifies the effect of friction, which in turn increases the stresses.

Now, the value of the friction coefficient μ expected for polystyrene spheres is about 0.4 at low rubbing speeds; for metal spheres, it could be lower, of order 0.3. The value of kμ can be found from matching the relative viscosity data with experiments at low (0.1 s^{-1}) shear rates made by Moon et al. (2015) at volume fractions of 0.4 and 0.5. We find that kμ ~ 0.70, and assuming $\mu = 0.4$, we find $k = 1.75$. Table 2 (last two columns) shows that the overall agreement of Eq. 3 with experiment is reasonable; it must be borne in mind that the data for the relative viscosities, both computed and experimental, and the values of P are subject to uncertainties of order 10%. Clearly, jamming will take place for ϕ in the range 0.5–0.6, although frictionless (bimodal) suspensions do not jam until $\phi \sim 0.66$ (Mari et al. 2014). The data in Table 2 suggest jamming occurs at $\phi \sim 0.57$. Random close packing indicates a divergence at $\phi = 0.639$ for monosized spheres, but with the bimodal system of Mari et al. (2014) and Cheal and Ness (2018), one expects (Qi and Tanner 2011) that the maximum packing fraction increases to about 0.665, close to the numerical result for frictionless spheres (0.66) reported by Mari et al. (2014).

Clearly, the relative viscosity is sensitive to the value assumed for the friction coefficient. For example, if μ is

Table 1 Computations of the relative viscosity (η_r^*) for frictionless spheres at various volume fractions

Source	Volume fraction (φ)		
	0.3	0.4	0.5
Sierou and Brady (2002)	3.10	6.24	15
Bertevas et al. (2010)	3.16	6.53	–
Mari et al. (2014)	~3.7	6.2	13.5
Gallier et al. (2014)	3.1	5.93	–
Cheal and Ness (2018)	–	5.68	13.1
Average	3.26	6.12	13.9

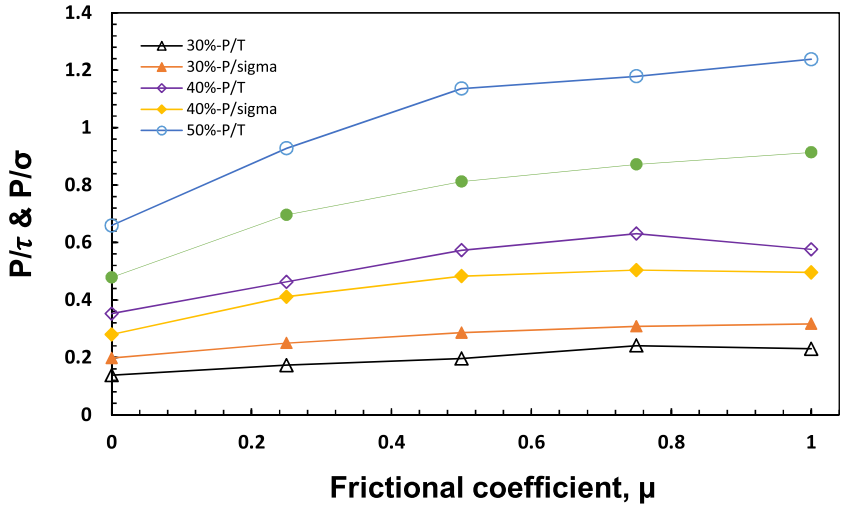

Fig. 1 The effects of frictional coefficient on P/τ and P/σ. The open symbols represent P/τ, the ratio of the particle pressure (P) to the shear stress (τ) in shear flow; the closed symbols represent P/σ, the ratio of the particle pressure (P) to the elongational stress (σ) in uniaxial elongational flow. The circles, diamonds, and triangles represent 50%, 40%, and 30% suspensions, respectively

increased by 5%, and k is kept constant, then the predicted η_r from Eq. 3 increases, for $\phi = 0.5$, from 55 to 65. The frictional rubbing speed also varies with shear rate—generally (Bowden and Tabor 1956; Moore 1975), an increase in shear rate gives a reduction in friction from the static value, down to a minimum, and then a rise at very large shear rates.

One might ask about changes in the values of P/τ due to other factors; they appear from the work of Sierou and Brady (2002) to be quite insensitive to assumed changes in interparticle forces (± 2% at $\phi = 0.4$). More data would clearly be welcome, but we will assume that P/τ is independent of these factors and depends only on the volume fraction and the friction coefficient.

Comparison with experiment

We can test these ideas against the extensive data of Thomas (1965). Thomas found considerable scatter in the results in the literature and proposed that a mean result for the relative viscosity was

$$\eta_r = 1 + 2.5\phi + 10.05\phi^2 + 0.00273\ \exp.(16.6\ \phi) \qquad (4)$$

Table 2 Suspension parameters for Eq. 3: $k = 1.75$, $\mu = 0.4$. Experiments at 0.1 s^{-1} from Moon et al. (2015). P/τ values for $\phi = 0.1$–0.2 from Sierou and Brady (2002); for $\phi = 0.3$ from Gallier et al. (2014); for 0.4 and 0.5 from Cheal and Ness (2018). The η_r^* average values for $\phi = 0.3$–0.5 are from Table 1 and for $\phi = 0.1$–0.2 from Sierou and Brady (2002)

ϕ	η_r^* (average)	P/τ	η_r (expt)	η_r (from Eq. 3)
0.1	1.33	0.0023	1.39	1.33
0.2	1.90	0.020	2.22	1.93
0.3	3.26	0.20	4.20	3.79
0.4	6.12	0.52	9.44	9.62
0.5	13.9	1.07	61.2	55.4

Results for the relative viscosity from Eq. (4) (Thomas) and Eq. (3) with kμ = 0.1 are shown in Table 3, together with the computed average frictionless η_r^* values from Table 2. The P/τ values assumed are for zero friction.

Clearly, the Thomas formula (Eq. (4)) is close to the frictionless result; if $k = 1.75$, then μ must have the low value of ~ 0.06. In fact, Thomas's data show a large scatter and the values found from Eq. (4) are not near the upper limits of η_r in Fig. 2; for example, at $\phi = 0.5$, Thomas showed that η_r ranges from 7.4 to 49.9. In Fig. 2, we compare the Thomas envelope (dashed lines) with the result of Eq. 4 and the data of column 4 in Table 3. The open black squares represent the computed frictionless results η_r^* in Fig. 2. Since the Thomas results do not recognize shear thinning, the scatter above and below the line of Eq. 4 is to be expected. Results with $\mu = 1$ lie close to the upper limits in Fig. 2.

A further investigation of the scheme can be made with the data of Moon et al. (2015) using a 1.1-Pa s silicone oil as a matrix fluid. There the roughness of the 40-μm diameter polystyrene spheres was reported—the average roughness was 0.15% of the sphere radius. The expected coefficient of dry friction at low rubbing speeds for this material is 0.4–0.5 (Bowden and Tabor 1956), but the friction coefficient is expected to fall at higher shear rates in the presence of fluid lubricant. Figure 3 shows the relative viscosity data as a

Table 3 Comparison with Thomas's (1965) data from Eq. 4 shown in column 2 and the results from Eq. 3 in column 4

ϕ	η_r (Eq. 4)	η_r^*	η_r (Eq. 3; kμ = 0.1)
0.1	1.36	1.33	1.32
0.2	1.98	1.90	1.90
0.3	3.05	3.26	3.32
0.4	5.70	6.12	6.34
0.5	15.75	13.9	14.9

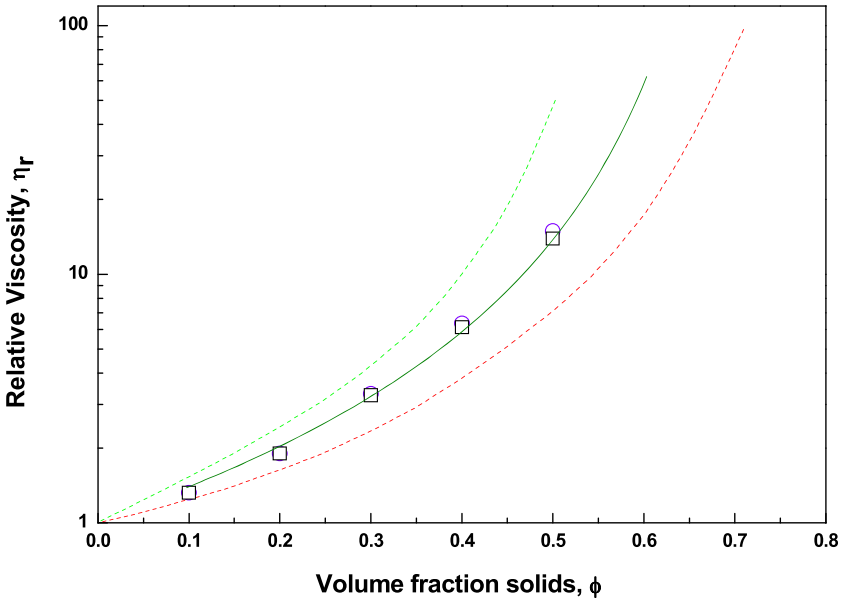

Fig. 2 Relative viscosity versus the volume fraction of the suspensions. In the figure, the dashed lines represent the upper and lower Thomas estimates. The full line presents Eq. 4. The black squares represent the frictionless relative viscosity from Table 2 column 2, and the values from Eq. 3 are shown as open circles

function of shear rate, and the shear thinning at higher concentrations is clear. This can be accounted for by assuming that kμ varies with shear rate; we will in fact assume that k is a fixed number (1.75), and all variation of kμ is due to variations of μ. Table 4 shows the experimental variation of η_r with shear rate in the range 0.1–100 s^{-1} for concentrations 0.1–0.5. The values of kμ at each shear rate were found from considering the values of η_r at $\phi = 0.4$ and 0.5. At the lowest rates of shearing, we assume $\mu = 0.4$ (at $\dot{\gamma} = 0.1\ s^{-1}$). Using $k = 1.75$, we find the values given in Tables 4 and 5. The relative viscosity data from Eq. 3 are presented in Fig. 3. It is probable that edge fracture is beginning at a shear rate of ~ 100 s^{-1} for $\phi = 0.5$. Keentok and Xue (1999) suggested from studies of polymer solutions that edge fracture occurred when $|N_2| > 5.5\Gamma/h$, where N_2 is the second normal stress difference, Γ is the surface tension coefficient, and h is the sample thickness at the rim. In the set of tests shown in Fig. 3 $\Gamma = 0.021$ Pa m, $h =$ 1 mm and from Dai et al. (2013) $N_2 = -4.4\,\phi^3\,\tau$, so for $\phi = 0.5$ and a shear rate of 100 s^{-1}, where the relative viscosity is 11.7 from Table 4 and the matrix viscosity is 1.1 Pa s, we find the magnitude of N_2 to be ~ 708 Pa, whereas the value of $5.5\Gamma/h$ is about 116 Pa. This suggests fracture does occur.

For comparison, the value of η_r found for polystyrene spheres by Boyer et al. (2011) from Eq. (2) is 31.9 for $\phi =$ 0.5. From Table 4, column 11, we see experimental values between 61.2 and 11.7, depending on shear rate. The value 31.9 lies between our data for shear rates of 1 and 10 s^{-1}.

The variation of μ with shear rate is indicative of less frequent solid-solid contact and/or better lubrication and is in accord with expectations (Bowden and Tabor 1956; Moore 1975). Of course, the actual shear rate between two spheres is higher than the macroscopic average shear rate, depending on the concentration ϕ (Vázquez-Quesada et al. 2017). Rough estimates of the amplification (M) of shear rate between

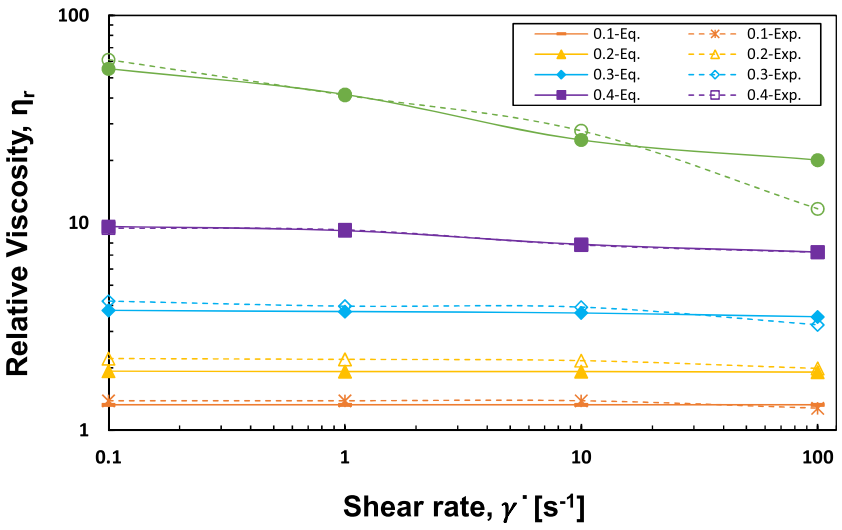

Fig. 3 Influence of shear rate on relative viscosity, showing shear thinning at higher concentrations. Dashed lines are experimental values; full lines are from Eq. 3 via Table 4. For the top curve ($\phi = 0.5$) at the largest shear rates, edge fracture occurs

Table 4 Relative viscosities at various shear rates for $\phi = 0.1$–0.5. Experimental values versus Eq. 3. $k = 1.75$, friction coefficients from Table 5

	$\phi = 0.1$		$\phi = 0.2$		$\phi = 0.3$		$\phi = 0.4$		$\phi = 0.5$	
$\dot{\gamma}$ (s^{-1})	Eq. 3	Exp.	Eq. 3	Exp.	Eq. 3	Exp.	Eq. 3	Exp.	Eq. 3	Exp.
0.1	1.33	1.39	1.93	2.22	3.79	4.2	9.61	9.44	55.4	61.2
1	1.33	1.39	1.92	2.2	3.74	3.97	9.18	9.26	41.6	41.3
10	1.33	1.39	1.92	2.17	3.68	3.93	7.88	7.83	25.1	27.8
100	1.33	1.28	1.91	1.99	3.53	3.23	7.24	7.22	20.1	11.7

particles have been given by Tanner and Dai (2016a); these are around 5 at $\phi = 0.3$, 8 at $\phi = 0.4$, and 19 at $\phi = 0.5$. (Ovarlez et al. (2015) have given another amplification factor (M*) which is of a similar order of magnitude.) Hence, even at small macroscopic shear rates, there are places of more intensive shear.

A further test of the bootstrap concept can be found from the work of Guy et al. (2015). That paper considers the viscosity of many sizes of polymethyl methacrylate (PMMA) spheres (0.268 to 45 μm diameter) in matrices with viscosities of 2.4 and 2.83 mPs s. In Fig. 1b of this paper, one sees two sets of results for high Péclet numbers (Pe)—the lower viscosity curve is very close to the frictionless results shown in Table 1 here, and the divergence of the viscosity is near random close packing ($\phi = 0.639$). The higher curve diverges at around $\phi = 0.56$. At $\phi = 0.5$, the higher curve shows a relative viscosity of 76.5, while the "frictionless" curve shows $\eta_r^* \sim$ 14.7 (Table 1 above shows 13.9). From Eq. 3, one finds, with $k = 1.75$ and $P/\tau = 1.07$ from Table 2, that $\mu = 0.43$, close to expectations. With this value of μ, the remaining data are described well.

It appears that the value of the friction coefficient is quite variable; some direct measurements of interparticle friction between two beads by Chatté et al. (2018) found, for polyvinyl chloride (PVC) spheres, that $\mu = 0.45 \pm 0.35$. Moore (1975) gives a friction coefficient of 0.4–0.5 for PVC.

Effect of particle roughness

One can also apply the model to the description of the effect of sphere roughness on relative viscosity. Experimental work by Moon et al. (2015) and Tanner and Dai (2016b) shows that sphere roughness increases the relative viscosity in suspensions with Newtonian matrices. We will assume that only the coefficient of friction changes with roughness. The roughness ratio is defined as (average roughness)/sphere radius. Tests with roughness ratios between 0.15 and 5.3% were carried out, and we report here only on the 0.15% and 5.3% results; the others show intermediate effects.

Hence, the relative viscosity η_{rough} becomes

$$\eta_{\text{rough}} = \frac{\eta_r^*}{\left[1 - k\mu_r\left(\frac{P}{\tau}\right)\right]} \tag{5}$$

where μ_r is the coefficient of friction for rough spheres. Using the data for 40-μm polystyrene spheres in a silicone oil matrix (1.1 Pa s viscosity at 24 °C) and assuming $k = 1.75$ as before, we find that the friction coefficient changes little until the shear rate approaches 10 s^{-1} or greater (Table 6).

There is generally a decrease of μ at higher shear rates. The last row of Table 6 shows the values of μ as a function of shear rate for the "smooth" spheres (actual roughness ratio ~0.15%) from Table 5. Edge fracture occurs at the highest shear rate for the 50% suspension, due to the large values of N_2, as discussed above.

Table 5 Values of k and μ for data of Fig. 3

$\dot{\gamma}$ (s^{-1})	kμ	k	μ
0.1	0.70	1.75	0.40
1	0.65	1.75	0.37
10	0.48	1.75	0.27
100	0.35	1.75	0.20

Table 6 Rough sphere friction coefficients for 5.3% roughness ratio (40-μm PS spheres) from Tanner and Dai (2016b)

ϕ	$\dot{\gamma}$ (s^{-1}) = 0.1	$\dot{\gamma}$ (s^{-1}) = 1	$\dot{\gamma}$ (s^{-1}) = 10	$\dot{\gamma}$ (s^{-1}) = 100
0.3	0.56	0.56	0.55	0.15
0.4	0.39	0.43	0.34	0.24
0.5	0.46	0.40	0.33	(fracture)
"Smooth" sph.	0.40	0.37	0.27	0.20

Uniaxial elongational flows

Although it is essential to consider flow types other than shearing in the study of suspension rheology (Mahmud et al. 2018), little has been done in this area. For example, in planar elongational flow, one has the computational work of Seto et al. (2017), and in uniaxial, planar, and biaxial elongation, Cheal and Ness (2018) have published extensive computations. In these computations, a steady state was achieved from

rest after a Hencky strain of around 1. There are no planar elongational experimental results to compare with the results of Seto et al. (2017), but the average pressure was given and it appears to be of the same order as the product of the matrix viscosity and the elongation rate. Importantly, for the bootstrap mechanism, P is positive.

Cheal and Ness (2018) have shown that frictionless uniaxial elongational suspension flows have a Trouton Ratio (Tr) of ~ 3, as in a pure Newtonian fluid. Larger values of Tr occurred when friction was introduced. Experiments by Mahmud et al. (2018) and Dai and Tanner (2017) show Tr values greater or less than 3.

In these necessarily unsteady in time elongational flows and also in unsteady shearing flows, one expects that the suspension structure, and hence η_r^* and P, also changes with time until it reaches a steady state. It seems that the bootstrap mechanism can be applied to study these steady states.

In steady uniaxial, planar, and biaxial extensional flows, let the extensional stress be σ and the corresponding extension rate be $\dot{\varepsilon}$. Then, the bootstrap analysis may be replicated to find

$$\sigma/\left(\eta_o\ \dot{\varepsilon}\right) = \frac{\eta_{re}^*}{\left[1-k_1\mu\left(\frac{P}{\sigma}\right)\right]} \tag{6}$$

where η_{re}^* is the relative frictionless viscosity value for the flow being considered. The constant k_1 is not expected to be the same as k for shearing. One can construct the Trouton ratio as follows.

$$T_r = \frac{\sigma}{\tau} = \frac{\eta_{re}^*\left[1-k\mu\left(\frac{P}{\tau}\right)\right]}{\eta_r^*\left[1-k_1\mu\left(\frac{P}{\sigma}\right)\right]} \tag{7}$$

Cheal and Ness (2018) found η_{re}^*/η_r^* to be nearly 3, 4, and 6 for uniaxial, planar, and biaxial extensions, respectively; these are the Newtonian values. For uniaxial flow, we can compare with the data of Dai and Tanner (2017).

In Table 7, the Trouton ratios (Tr) are computed using the average of the experimental relative viscosity values and the shear results from Table 2. As shown by Mahmud et al. (2018), the Trouton ratio values vary considerably. While the agreement between experiment and calculation is reasonable, it is necessary to postulate a higher friction coefficient for $\phi = 0.3$ and 0.4. The only other experimental data (Mahmud et al. 2018) show considerably smaller viscosities at larger strain rates. The viscosity values for $\phi = 0.3$ and 0.4 fall below the frictionless computed values, which indicates that strain-rate thinning occurs. The cause of this is not known; it is not due to the mechanism proposed by Vázquez-Quesada et al. (2017) where the shear thinning of the matrix fluid is considered. For the suspensions, it is expected that the rates of deformation between spheres are around $8\sqrt{3}$ times the maximum elongation rate; this, for $\phi = 0.4$, is about 560 s^{-1}. From Vázquez-Quesada et al. (2017), one finds that the silicone oil matrix viscosity will drop by about 12% at this rate of deformation. However, the elongational relative viscosities measured by Mahmud et al. (2018) are only about 9.5, whereas the frictionless computations give 16.8.

Table 7 Uniaxial extension results. P/σ and viscosity data from Cheal and Ness (2018); $k = 1.75$, $k_1 = 2.7$. Experiments from Dai and Tanner (2017) at elongation rates of 0.6–2.3 s^{-1}

ϕ	μ	η_{re} (expt)	η_{re} (Eq. 6)	Tr (calc)	Tr (expts)
0.3	0.45	14–20	14.9	4.0	4.3
0.4	0.45	36–55	41.1	4.5	4.9
0.5	0.35	92–147	127	3.0	2.9

The odd behavior with corn syrup matrices

The work of Tanner and Dai (2016a) showed that suspensions with corn syrup-based matrices exhibited huge unexpected increases in relative viscosities when the spheres were roughened. Using the same 40-μm diameter spheres as in the work above (Dai and Tanner 2017), experiments with pure corn syrup and Boger fluid matrices were made. At 24 °C, the corn syrup showed a constant viscosity of 3.66 Pa s in a shear rate range of 0.1 to 1000 s^{-1}; normal stresses were too small to measure. In order to get consistent results, it was necessary to prevent evaporation and consequent crusting at the rim of the samples. With "smooth" (actually 0.15% roughness ratio) spheres, the results were much as expected, but for rougher spheres (roughness ratio of 5.3%), very large unexpected increases of relative viscosity were seen at low shear rates (0.1 s^{-1}) while at larger shear rates, up to 100 s^{-1} severe shear thinning was seen (Fig. 4).

Tests were also made with a Boger fluid made up with 79.24% by weight of corn syrup and 19.80% glycerine and with the addition of a mixture of water and polyacrylic acid (PAA). This recipe is similar to that used by Zarraga et al. (2001) and Dai et al. (2014). The addition of the glycerine, which absorbs water from the atmosphere, helps counteract the tendency of the corn syrup to dry out. The mixture exhibits a nearly constant viscosity of 2.15 Pa s over the range 0.1–100 s^{-1} in shear rate. Because of the PAA, measurable normal stresses were present. Figure 5a, b shows the relative viscosity results for $\phi = 0.3$ and 0.4 for the Boger fluid suspensions. In both cases, the large increase of relative viscosity seen at 0.1 s^{-1} disappears at 100 s^{-1}; here, the relative viscosities for "smooth" and rough spheres coincide. We can use the bootstrap idea to study this behaviour.

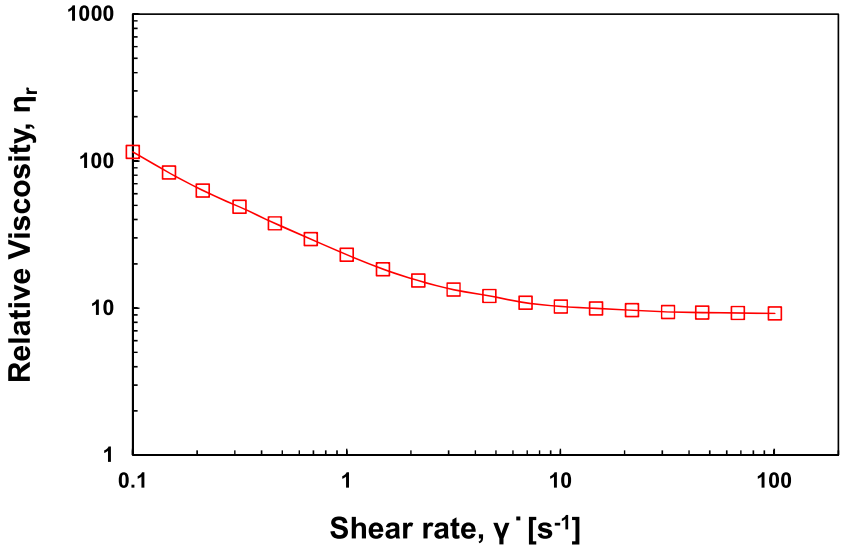

Fig. 4 Effects of shear rate on relative viscosity for 40% volume fraction suspensions of 40-μm PS spheres in corn syrup. Sphere roughness ratio 5.3%

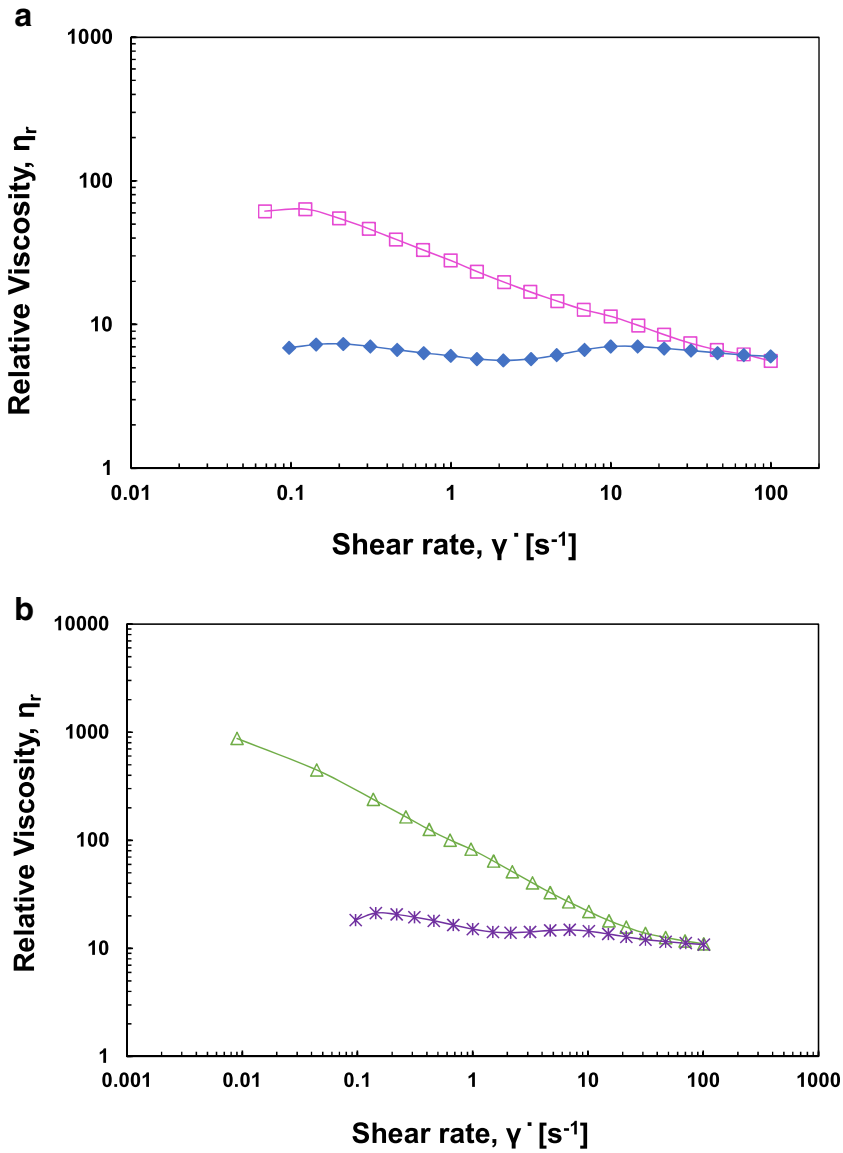

Fig. 5 **a** Relative viscosity comparisons between 30% volume fraction "smooth" and rough spheres in syrup-glycerin-4%PAA/water Boger fluid. 30% 40-μm PS 0.15% roughness (diamonds); 30% 40-μm PS (roughness ratio 5.3%) (squares). **b** Relative viscosity comparison. 40% 40-μm PS (5.3% roughness)-syrup-glycerin-4%PAA/water (triangles); 40% 40-μm PS (0.15% rough) in syrup-glycerin-4%PAA/water Boger fluid (asterisks)

Table 8 Friction coefficients for polystyrene spheres

Matrix	ϕ	Roughness (%)	μ (0.1 s^{-1})	μ (100 s^{-1})
Corn syrup	0.4	5.3	0.95	0.37
Silicone oil	0.4	0.15	0.40	0.20
Silicone oil	0.4	5.3	0.39	0.24
Boger fluid	0.3	0.15	1.00	0.88
Boger fluid	0.3	5.3	1.41	0.88
Boger fluid	0.4	0.15	0.68	0.41
Boger fluid	0.4	5.3	0.98	0.41
PS dry friction	–	–	0.4–0.5	0.4–0.5

We assume that $k = 1.75$ remains unchanged in Eq. 3 and that the frictionless relative viscosity (η_r^*) and the mean pressure factor (P/τ) remain as in Table 2. Then, we can compute the friction coefficient μ needed to describe the corn syrup results (Table 8).

Discussion

So far, no scaling of the deformation rate has been given. We plot the friction coefficients for the Newtonian cases from Tables 5 and 6 in Fig. 6. The dry friction line ($\mu = 0.45$) is also shown. The data indicate that the friction coefficients begin to decline at a shear rate of order 1 s^{-1}.

Considering that the rotation rate of the spheres is a fraction of $\dot{\gamma}$, then the relative rubbing speed is of order $\dot{\gamma}a$, where a is the sphere radius. The magnitude of this rubbing speed in the experiments quoted in Fig. 3, where $a = 20$ μm, varies from 2 μm/s at a shear rate of 0.1 s^{-1} up to 2 mm/s at a shear rate of 100 s^{-1}. Hence, it is suggested that the critical rubbing speed (U_c) for the onset of lower friction is about 20 μm/s. Using this value, all of the previous data can be plotted in a dimensionless manner.

The rough spheres in Table 6 have friction coefficients comparable to the Boyer et al. formula in Eq. 1 above; their friction coefficient μ^c varies from 0.7 at $\phi = 0$ down to 0.64 at $\phi = 0.5$. The high friction coefficient for the corn syrup matrix in Table 8 at low shear rates is surprising. It is not expected that corn syrup will crystallize, but something like gelling must be taking place.

The results for the Boger fluids (Table 8), which also show high μ values, indicate that for these non-Newtonian matrices, additional factors are in play; it is likely that the frictionless viscosities are variable and it is unlikely that k is a constant. Unfortunately, there are no computations to illuminate these points at present.

As for the elongational results, the marked strain-rate thinning seen by Mahmud et al. (2018) remains to be further explored.

Conclusion

The bootstrap mechanism of friction enhancement in non-colloidal suspensions appears to be a useful idea; the needed parameters (η_r^*) and the mean pressure factor (P/τ) can be computed, but are not known very precisely. Assuming k is fixed at 1.75, then reasonable values of the friction coefficient between the spheres can be deduced for many of the Newtonian matrix suspensions. We note the need for further accurate, self-consistent computer modeling with realistic friction models; it appears that constant friction coefficients are inadequate.

We have tested the idea with the Thomas (1965) data, which do not consider shear thinning explicitly and with our own data (Moon et al. 2015) for 40-μm diameter polystyrene spheres in silicone oil (viscosity 1.1 Pa s); the data of Guy et al. (2015) were also used. Volume fractions up to 0.5 were considered. In order to introduce shear thinning, the friction coefficients are assumed to be a function of sliding speed (U).

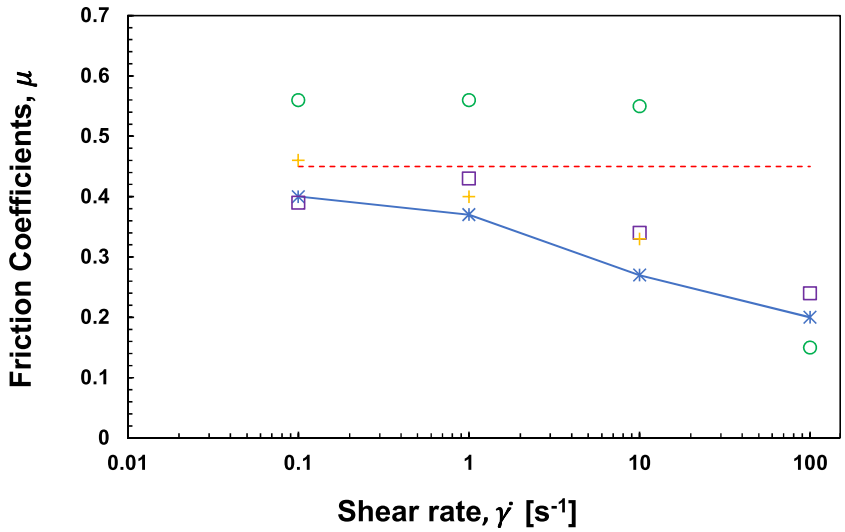

Fig. 6 Variations of friction coefficients with shear rate. The horizontal dotted line is the value for polystyrene (~0.45). The circles, squares, and plus signs are for rough spheres of 30, 40, and 50% concentration from Table 6; the solid line gives the data for "smooth" spheres from Table 5

In the present case, the critical sliding speed (U_c) appears to be about 20 μm/s, and friction coefficients appear to drop when this rate is exceeded. (There are other suggested mechanisms of shear thinning available—for example see Vásquez-Quesada et al. (2017) and Kroupa et al. (2017), but these effects are assumed not to be dominant here.) The introduction of roughness is considered; there is an increase of relative viscosity with increasing roughness due to increasing friction coefficients. For corn syrup-based matrices, we show that the results can be explained by large friction coefficients at low shear rates ($0.1\ s^{-1}$), while at higher ($100\ s^{-1}$) shear rates, these unusual effects disappear. The very large friction coefficient with the Boger fluid indicates that a further analysis is needed, taking account of normal stress or other viscoelastic effects.

With the Newtonian matrices, the values of the first and second normal stress differences are proportional to the shear stress (Zarraga et al. 2000; Dai et al. 2013), so the complete set of viscometric data can be found when the shear stress is known.

Finally, it appears that non-viscometric flows, such as elongation, can be considered with the model, but more computations and experiments are needed.

Acknowledgements We thank the University of Sydney for providing scholarship support for Arif Mahmud. JiYoung Moon acknowledges that his research was supported by the Basic Science Research Program of the National Research Foundation of Korea (NRF) funded by the Ministry of Education (2017R1A6A3A03003276). C.N. acknowledges financial support from the Maudslay-Butler Research Fellowship at Pembroke College, Cambridge.

References

Bertevas E, Fan XJ, Tanner RI (2010) Simulation of the rheological properties of suspensions of oblate spheroidal particles in a Newtonian fluid. Rheol Acta 49:53–73

Bowden FP, Tabor D (1956) Friction and lubrication. Methuen, London

Boyer F, Guazzelli É, Pouliquen O (2011) Unifying suspension and granular rheology. Phys. Rev. Letters 107:art 188301

Chatté G, Comtet J, Nigues A, Bocquet L, Siria A, Ducouret G, Lequeux F, Lenoir N, Ovarlez G, Colin A (2018) Shear-thinning in non-Brownian suspensions. Soft Matter 14:879–893

Cheal O, Ness C (2018) Rheology of dense granular suspensions under extensional flow. J Rheol 62:501–512

Dai SC, Tanner RI (2017) Elongational flows of some non-colloidal suspensions. Rheol Acta 56:63–71

Dai SC, Bertevas E, Qi F, Tanner RI (2013) Viscometric functions for non-colloidal sphere suspensions with Newtonian matrices. J Rheol 57:493–510

Dai SC, Qi F, Tanner RI (2014) Viscometric functions of concentrated non-colloidal suspensions of spheres in a viscoelastic matrix. J Rheol 58:183–198

Gallier S, Lemaire E, Peters F, Lobry L (2014) Rheology of sheared suspensions of rough frictional particles. J Fluid Mech 757: 514–549

Guy BM, Hermes M, Poon WCK (2015) Towards a unified description of the rheology of hard-particle suspensions. Phys. Rev. Lett 115:art 088304

Huang N, Ovarlez G, Bertrand F, Rodts S, Coussot P, Bonn D (2005) Flow of wet granular materials. Phys Rev Lett 94:028301

Keentok M, Xue SC (1999) Edge fracture in cone-plate and parallel plate flows. Rheol Acta 38:321–348

Kroupa M, Soos M, Kosek J (2017) Slip on a particle surface as the possible origin of shear thinning in non-Brownian suspensions. Phys Chem Chem Phys 19:5979–5984

Mahmud A, Dai SC, Tanner RI (2018) A quest for a model of non-colloidal suspensions with Newtonian matrices. Rheol Acta 57: 29–41

Mari R, Seto R, Morris JF, Denn MM (2014) Shear thickening, frictional and frictionless rheologies in non-Brownian suspensions. J Rheol 58:1693–1724

Moon JY, Dai SC, Chang L, Lee JS, Tanner RI (2015) The effect of sphere roughness on the rheology of concentrated suspensions. J Non- Newt Fluid Mech 223:233–239

Moore DF (1975) Principles and applications of tribology. Pergamon Press, Oxford

Ovarlez G, Mahaut F, Deboeuf S, Lenoir N, Hormozi S, Chateau X (2015) Flows of suspensions of particles in yield stress fluids. J Rheol 59:1449–1486

Qi F, Tanner RI (2011) Relative viscosity of bimodal suspensions. Korea-Australia Rheology J 23:105–111

Seto R, Giusteri GG, Martinello A (2017) Microstructure and thickening of dense suspensions under extensional and shear flows. J Fluid Mech Rapids 825:art. R3

Sierou A, Brady JF (2002) Rheology and microstructure in concentrated noncolloidal suspensions. J Rheol 46:1031–1056

Tanner RI, Dai SC (2016a) Rheology of non-colloidal suspensions with corn syrup matrices. Rheol Acta 55:739–747

Tanner RI, Dai SC (2016b) Particle roughness and rheology in noncolloidal suspensions. J Rheol 60:809–818

Thomas DG (1965) Transport characteristics of suspension: VIII. A note on the viscosity of Newtonian suspensions of uniform spherical particles. J Colloid Sci 20:267–277

Vázquez-Quesada A, Mahmud A, Dai SC, Ellero M, Tanner RI (2017) Investigating the causes of shear-thinning in non-colloidal suspensions. J. Non- Newt. Fluid Mech. 248:1–7

Zarraga IE, Hill DA, Leighton DT (2000) The characterization of the total stress of concentrated suspensions of noncolloidal spheres in Newtonian fluids. J Rheol 44:185–220

Zarraga IE, Hill DA, Leighton DT (2001) Normal stress and free surface deformation in concentrated suspensions of noncolloidal spheres in a viscoelastic fluid. J Rheol 45:1065–1084